

Relaxation and Readout Visibility of a Singlet-Triplet Qubit in an Overhauser Field Gradient

C. Barthel^{1,*}, J. Medford^{1,*}, H. Bluhm^{1,†}, A. Yacoby¹, C. M. Marcus¹, M. P. Hanson², and A. C. Gossard²

¹*Department of Physics, Harvard University,
Cambridge, Massachusetts 02138, USA*

²*Materials Department, University of California,
Santa Barbara, California 93106, USA*

Using single-shot charge detection in a GaAs double quantum dot, we investigate spin relaxation time (T_1) and readout visibility of a two-electron singlet-triplet qubit following single-electron dynamic nuclear polarization (DNP). For magnetic fields up to 2 T, the DNP cycle is in all cases found to increase Overhauser field gradients, which in turn decrease T_1 and consequently reduce readout visibility. This effect was previously attributed to a suppression of singlet-triplet dephasing under a similar DNP cycle. A model describing relaxation after singlet-triplet mixing agrees well with experiment. Effects of pulse bandwidth on visibility are also investigated.

PACS numbers:

I. INTRODUCTION

Confined few-electron systems are of interest for exploring spin coherence and controlled entanglement,¹ as probes of mesoscopic nuclear spin environments,^{2,3} and as qubits for quantum information processing.^{4,5} The singlet-triplet basis of two electron spins in a double quantum dot has been widely investigated as a qubit with immunity to dephasing from fluctuating uniform magnetic fields.⁶ An important source of both spin dephasing and relaxation in GaAs devices is hyperfine coupling to nuclear spins in the host material. The slow evolution of longitudinal Overhauser fields allows echo techniques to recover phase coherence^{7–9}, while even static gradients of Overhauser fields can induce triplet-to-singlet relaxation,¹⁰ limiting readout fidelity.¹¹ It is therefore important to understand how gradients in local Zeeman fields, either from micromagnets^{12,13} or Overhauser fields,¹⁴ affect singlet-triplet qubit relaxation, particularly during readout.

Dynamic nuclear polarization (DNP) using cyclic single-spin transitions can transfer angular momentum from electrons in the double dot (refreshed from reservoirs) into the host nuclear system, inducing a net nuclear polarization.^{14–16} In Ref. 17, it was observed that for tens of seconds following the application of the DNP cycle, the probability, P_S , to measure a singlet outcome, after allowing a prepared singlet to evolve in separate dots, remained close to unity. This surprising observation was interpreted as the DNP cycle having reduced the difference in Overhauser fields between the two dots below the normal (thermal) fluctuation level while inducing a net polarization. That interpretation was consistent with some theoretical results,^{19–21} but at odds with subsequent experiment¹⁴ and more recent theory.²²

In this paper, we show that over a broad range of applied magnetic fields, the DNP pumping cycle investigated in Refs. 14–17 enhances rather than reduces the

gradient in nuclear polarization, along with inducing an average polarization. Rapidly repeated single-shot readout¹¹ reveals that the enhanced nuclear gradient leads to a reduction in the visibility of qubit precession. We investigate qubit readout visibility as a function of nuclear field gradient, applied magnetic field, and gate voltage configuration during the measurement step of a cyclic pulse sequence. Simultaneously, triplet relaxation at the measurement point is measured in the time domain, taking advantage of fast readout electronics. We find that the dominant reduction in visibility for large nuclear polarizations is due to increased relaxation of the $m = 0$ triplet during measurement, independent of applied magnetic field. We develop a model describing triplet decay via charge relaxation after rapid singlet-triplet mixing driven by a Zeeman field difference between dots, including effects of finite pulse bandwidth. The model is found to be in very good agreement with experimental results. These results suggest an alternative interpretation of the increased singlet measurement probability following DNP,¹⁷ which is that the enhanced nuclear field gradient induced by DNP causes rapid relaxation of the triplet state during measurement, which in turn diminishes measurement visibility while the nuclei are out of equilibrium.

The remainder of the paper is organized as follows. Section II describes the double dot system and the experimental setup. The theory of the two-electron qubit system and nuclear pumping is briefly reviewed in the first part of section III. The second part of section III discusses mechanisms of spin relaxation during measurement and introduces a model of these effects. Experimental results are presented in section IV, beginning with the measurement of nuclear gradients and precession visibilities. Observed connections between visibility, relaxation time and Overhauser field difference are then presented, along with data showing the influence of limited pulse bandwidth. A summary of results and conclusions are given in section V.

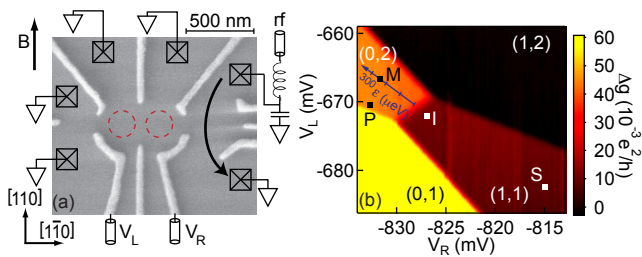


FIG. 1: (a) (Color online) (a) Micrograph of device lithographically identical to the one measured. Gate voltages, V_L and V_R , set the electrostatic energy of left and right dot. A sensor quantum dot on the right allows fast measurement of the double dot charge state via rf reflectometry. The direction of applied magnetic field, B , is indicated, as well as the GaAs crystal axes. (b) Change of sensor dc conductance Δg , with double dot charge state (N_L, N_R), constrained to (1,1), (0,2) in this work. The qubit state is controlled by the (1,1)-(0,2) energy detuning, ϵ , set by gate voltages V_L and V_R along the diagonal axis through the markers S, M. The scaling of detuning is $|\epsilon| = \eta \sqrt{\Delta V_L^2 + \Delta V_R^2}$, with a lever arm $\eta = 40 \mu\text{eV/mV}$ and voltage detunings, $\Delta V_L, \Delta V_R$, from the (1,1)-(0,2) charge degeneracy.²³ Markers indicate gate voltages during pump-and probe-cycles. Singlet preparation at point P. Pump: $S-T_+$ mixing at point I, see text. Probe: Separation of singlet for $S-T_0$ mixing at point S and measurement at point M at variable detuning, $80 \mu\text{eV} < \epsilon_M < 260 \mu\text{eV}$.

II. SYSTEM

Double quantum dots were formed by Ti/Au depletion gates on a GaAs/Al_{0.3}Ga_{0.7}As heterostructure with a two-dimensional electron gas (2DEG) of density $2 \times 10^{15} \text{ m}^{-2}$ and mobility $20 \text{ m}^2/\text{Vs}$, 100 nm below the wafer surface. Except where noted, a field of 200 mT was applied in the direction shown in Fig. 1(a) using a vector magnet. Measurements were performed in six cool-downs of four devices for magnetic fields along all three crystal axes [Fig. 1(a)] over a range of applied magnetic fields from 10 mT to 2 T. The same overall phenomenology was found in all measurements. Results are reported here for one of those devices.

A proximal radio-frequency sensor quantum dot (SQD) [Fig. 1(a)] was used to sense the charge state of the double dot.^{24,25} Reflectometry measurement on the SQD provides an output voltage, v_{rf} , with good signal-to-noise on sub- μs time scales.²⁴ The SQD was energized only during readout to avoid disturbance during gate operations. Gate voltages V_L and V_R , pulsed using a Tektronix AWG5014, controlled charge occupancies N_L and N_R of the left and right dots. The charge state (N_L, N_R) was restricted to (1,1) and (0,2), and was controlled by gate voltages along an axis of energy detuning, ϵ , running between separation (S) and measurement (M) points [Fig. 1(b)]. Detuning scales as $|\epsilon| = \eta \sqrt{\Delta V_L^2 + \Delta V_R^2}$, where ΔV_L and ΔV_R are gate voltages relative to the charge transition point, and $\eta = 40 \mu\text{eV/mV}$ is the voltage-to-energy lever arm, calibrated via transport

through the double dot.^{23,26,27} Note that the two gates contribute symmetrically to detuning, as observed experimentally. The influence of V_L and V_R on the interdot tunnel coupling is found to be small for the range of voltages used, and is neglected in the model presented below.

III. MODEL

The dependence of the two-electron energy levels on detuning, ϵ , is shown in Fig. 2(a) for the regime relevant to singlet-triplet qubit operation. The two-level system that forms the qubit is the two-electron singlet, S , and the $m = 0$ triplet, T_0 , of the (1,1) charge state. Preparation of the S state is achieved through relaxation into the (0,2) singlet state via electron exchange with the leads at point P [see Figs. 1(b) and 2(a)]. The (0,2) singlet can be separated into the (1,1) singlet, S , ($+z$ on the qubit Bloch sphere) by following the lower branch of the singlet anticrossing through $\epsilon = 0$ [anticrossing of black curves in Fig. 2(a)].

A net polarization of nuclei in the host GaAs substrate in the vicinity of the double quantum dot can be created electrically by cycling ϵ through the anticrossing of the singlet S and the $m = 1$ triplet, T_+ , at point I [inset of Fig. 2(a)].^{14–17} First, moving slowly through the anticrossing, an electron spin is flipped and a nuclear spin is flopped via hyperfine interaction. The system is then quickly brought to $\epsilon > 0$, without spin flip, and is reset to a singlet state at P via electron exchange with the leads. Ideally, the nuclear pumping cycle flips one nuclear spin per cycle but in practice the efficiency is typically lower.¹⁸

In an applied magnetic field, \mathbf{B} , whose direction defines the z direction in real space, qubit states at the separation point, S, are split by the *difference* in the z components of Zeeman fields (including nuclear Overhauser fields), ΔB_z , between left and right dots. This causes a precession between S and T_0 at frequency

$$f_S = \frac{|g| \mu_B \Delta B_z}{h}, \quad (1)$$

where h is Planck's constant, μ_B is the Bohr magneton, and $g \sim -0.4$ is the electron g -factor in GaAs. A frequency shift away from f_S due to residual exchange at the separation point, $J_S \sim 10 \text{ neV}$ ($\sim 0.5 \text{ mT}$), is usually much smaller than $g\mu_B \Delta B_z$ in the present experiments. A nonvanishing J_S also reduces readout visibility,

$$V_J = \frac{\Delta B_z^2}{\Delta B_z^2 + (J_S/g^* \mu_B)^2} < 1, \quad (2)$$

as previously shown theoretically³⁰ and experimentally.³¹ In this work, however, $V_J \sim 1$; the reduced visibility arises from other sources, as discussed below.

The sensitivity of qubit relaxation and readout visibility to gradients in Overhauser fields was investigated using a probe cycle following a sequence of DNP cycles.^{3,11,14} The probe cycle prepares a spin singlet in

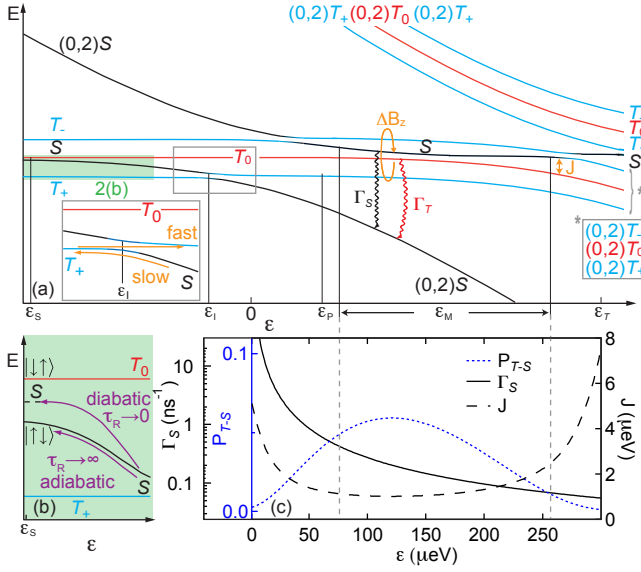


FIG. 2: (a) (Color online) (a) Energy level diagram as function of detuning, ϵ , for the (1,1) charge state except where noted. Pulse-cycle detunings, ϵ_P of singlet preparation, ϵ_1 of S - T_+ resonance, and ϵ_S of S - T_0 precession, are labeled. The relaxation channels of triplet state, T_0 , during measurement at ϵ_M are indicated: Charge relaxation, Γ_S , after S - T_0 mixing by nuclear field difference, ΔB_z , and processes not involving ΔB_z , at rate Γ_T . The S - T_0 mixing is suppressed by the exchange energy splitting, J , due to two anticrossings, at $\epsilon = 0$ between singlet states of (1,1)-(0,2), and at $\epsilon = \epsilon_T \sim 300 \mu\text{eV}$ between triplet states of (1,1)-(0,2). Inset: Pump cycle around S - T_+ anticrossing at ϵ_1 . (b) Ramping detuning to ϵ_S over a time τ_R converts an initial S into an admixture of S and $|\uparrow\downarrow\rangle$ with amplitudes that depend on τ_R . (c) Charge relaxation rate, Γ_S , of metastable S state [Eq. (9)]; singlet probability, P_{T-S} , from admixture [Eq. (5)]; exchange J [Eq. (6)], as functions of detuning, ϵ using experimental parameters (see text).

(0,2), separates to point S for a time τ_S , then returns to the measurement point M . If the two electrons are in a singlet configuration, they return to (0,2); if they are in a triplet configuration, they remain in (1,1). Superpositions are projected to one of the two charge states during measurement. Spin-to-charge conversion requires the measurement time be shorter than the relaxation time of the metastable triplet to the (0,2) singlet.

The probability of measuring a singlet or a triplet was determined by accumulating statistics of multiple single-shot measurements.¹¹ When the single-shot integration time τ_M was much shorter than T_1 , the distribution of outcomes formed two separated, noise-broadened Gaussians centered at the amplitudes corresponding to singlet (v_{rf}^S) and triplet (v_{rf}^T) states. Measurement visibility can be expressed as $V_M = F_S + F_T(T_1) - 1$, where F_S (F_T) is the singlet (triplet) fidelity, corresponding to the probability that a singlet (triplet) is correctly identified as such.¹¹ Depending on the ratio τ_M/T_1 , the metastable triplet may decay into a singlet during the measurement,

leading to overcounting of singlets and undercounting of triplets in the output distribution.¹¹ Specifically—and this is a key point of our analysis—for fixed measurement time, τ_M , the measurement visibility V_M decreases with decreasing T_1 . We note that the same reduction in visibility will be observed for time averaged readout—as opposed to single-shot readout—as was used in Refs. 7,17.

To measure relaxation of triplet states into singlets during measurement, $v_{\text{rf}}(t)$ was measured with high temporal resolution after moving to point M , then subsequently averaged over many successive pulse cycles. For short measurement times, $t \ll T_1$, the signal corresponds to an equal mix of singlet and triplet states, $\langle v_{\text{rf}}(t) \rangle \sim (v_{\text{rf}}^S + v_{\text{rf}}^T)/2$, while for $t \gg T_1$ the signal corresponds to the (0,2) charge state and therefore the singlet, $\langle v_{\text{rf}}(t) \rangle \sim v_{\text{rf}}^S$. Experimentally, we find that $\langle v_{\text{rf}}(t) \rangle$ is approximately exponential in t , giving a measure of the triplet relaxation time T_1 at the measurement point.

Relaxation pathways of the $m = 0$ triplet at M are shown in the energy diagram in Fig. 2(a). A difference in Zeeman fields, ΔB_z , between the two dots will cause rapid precession between T_0 and the (1,1) singlet, S , which can then rapidly relax to the (0,2) singlet with a rate Γ_S via spin-conserving phonon emission. Direct relaxation of the (1,1) triplet, at a rate Γ_T , involves a change in total spin—mediated, for instance, by electron exchange with the leads—and so is a much slower process.

In previous measurements of triplet relaxation, exchange, J , at point M [see Fig. 2(a)] was intentionally set to be much smaller than ΔB_z .¹⁰ In that case, a T_0 state brought to M would oscillate between S and T_0 rapidly, giving an average singlet occupation of 1/2, and a decay rate $\Gamma_S/2$, independent of ΔB_z . In the present measurement as well as in previous T_2^* -type experiments^{7,14,17}, tunnel coupling is much larger, so that J at point M is not necessarily small compared to ΔB_z . The effect of sizable J at the measurement point is a suppression of mixing between T_0 and S by an amount that depends on the ratio $\Delta B_z/J$. In this case, the average S occupation at M , and thus triplet decay via fast spin-conserving processes, will increase with increasing ΔB_z .

Triplet decay is modeled by extending Ref. 28 to include nonzero J . Populations of the eigenstates of the Hamiltonian $\mathcal{H} = J(\epsilon_M)(\sigma_z + \mathbb{I})/2 - \Delta B_z \sigma_x/2$, decay with rates $\Gamma^\pm = \Gamma_S(\epsilon_M)|\langle S|E^\pm\rangle|^2 + \Gamma_T|\langle T_0|E^\pm\rangle|^2$.

The eigenstates of \mathcal{H} are given by

$$|E^\pm\rangle = \frac{\Delta B_z|S\rangle + \Omega^\pm|T_0\rangle}{\sqrt{\Delta B_z^2 + (\Omega^\pm)^2}}, \quad (3)$$

where $\Omega^\pm = J(\epsilon_M) \pm \sqrt{J^2(\epsilon_M) + \Delta B_z^2}$.

In principle, this results in a bi-exponential decay of the triplet probability, $P_T(t) = P_T(0)(|\langle T_0|E^+\rangle|^2 e^{-t\Gamma^+} + |\langle T_0|E^-\rangle|^2 e^{-t\Gamma^-})$, but in practice, we expect only a single exponential. This is due to the fact that for $J \gg \Delta B_z$, $|E^-\rangle$ has a large overlap with the singlet, leading to a much larger Γ^- and a correspondingly small overlap with T_0 . For instance, for large nuclear gradients,

$\Delta B_z \sim 35$ mT, and small exchange splittings, $J \sim 1$ μ eV, $|E^- \rangle$ accounts for roughly one eighth of the initial triplet, and decays seven times more rapidly than the triplet-like eigenstate, $|E^+ \rangle$. Under such conditions, we can model $P_T(t)$ as a single exponential, $P_T(0)e^{-t/T_1}$, where

$$T_1 = (\Gamma^+)^{-1} \cong [\Gamma_S(\epsilon_M)P_{T-S} + (1 - P_{T-S})\Gamma_T]^{-1}, \quad (4)$$

and P_{T-S} is the fraction of the remaining triplet that overlaps with the (1,1) singlet,

$$P_{T-S} = |\langle S|E^+ \rangle|^2 = \frac{1}{2} \left(1 - \frac{J(\epsilon_M)}{\sqrt{\Delta B_z^2 + J(\epsilon_M)^2}} \right). \quad (5)$$

In this model, Γ_T is governed by a decay channel that is independent of ΔB_z , such as exchange with the leads. In principle, non-spin-conserving processes that generate triplet relaxation also contribute to Γ_S , but since Γ_T is at least two orders of magnitude smaller than Γ_S for all ϵ_M in the experiment, these contributions can be neglected. To simplify the modeling further, we assume Γ_T does not depend on ϵ_M .

Exchange splitting at the measurement point, $J(\epsilon_M)$, is affected by two charge-state anticrossings, one of the (0,2) and (1,1) singlet states, centered at $\epsilon = 0$, and the other of the (0,2) and (1,1) T_0 states, centered at $\epsilon = \epsilon_T$ [see Fig. 2(a)]. For $0 < \epsilon_M < \epsilon_T$, the (1,1) singlet is the upper branch (denoted \cup) of the singlet anticrossing, and the (1,1) triplet is the lower branch (denoted \cap) of the T_0 anticrossing. Also, in this range the upper branch of the singlet anticrossing remains above the lower branch of the T_0 anticrossing. We write

$$J(\epsilon_M) = E_S(\epsilon_M) - E_{T_0}(\epsilon_M) \quad (6)$$

using the forms given in Eqs. (16,17) in Ref. 28.²⁹ The singlet energy is

$$E_S(\epsilon) = E_{\cup}(\epsilon) = \frac{t_S^2}{\sqrt{4t_S^2 + \epsilon^2} + \epsilon}, \quad (7)$$

where t_S is the tunnel coupling for the singlet anticrossing centered at $\epsilon = 0$, and the triplet energy is

$$E_{T_0}(\epsilon) = E_{\cap}(\epsilon - \epsilon_T) = \frac{-t_T^2}{\sqrt{4t_T^2 + (\epsilon - \epsilon_T)^2} - (\epsilon - \epsilon_T)}, \quad (8)$$

where t_T is the tunnel coupling for the T_0 anticrossing centered at $\epsilon = \epsilon_T$.

In previous experiments, Γ_S was found to decrease with increasing detuning with a dependence falling between ϵ^{-1} and ϵ^{-2} , consistent with expected phonon mechanisms.³³ Specifically, piezoelectric interaction with 3D (2D) phonons gives $\Gamma_S \propto \epsilon^{-1}$ (ϵ^{-2}).³³ Here, we assume a form

$$\Gamma_S = \alpha\epsilon^{-1} + \beta\epsilon^{-2}, \quad (9)$$

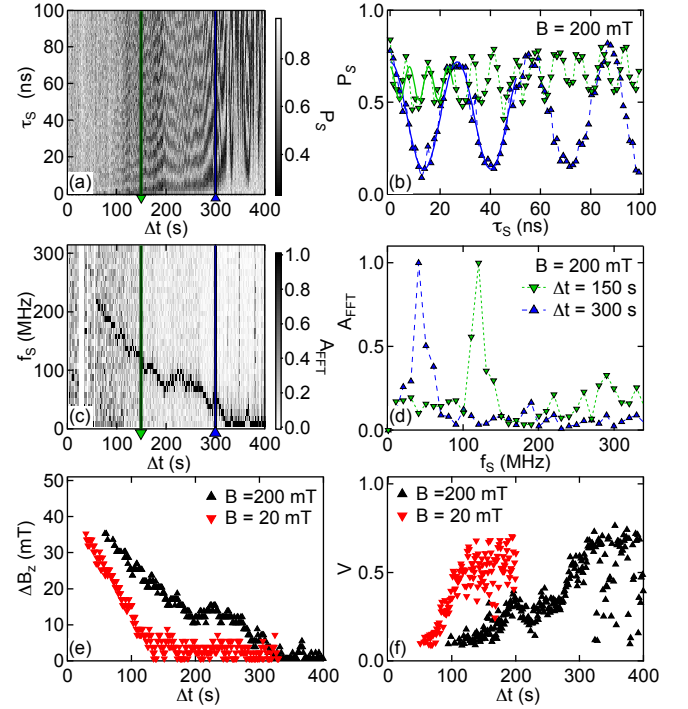


FIG. 3: (Color online) (a) Probability, P_S , of singlet measurement outcome (grayscale) as function of S - T_0 mixing time, τ_S , and time, Δt , after a 60 s, ~ 4 MHz pump cycle; taken at $B = 200$ mT. Note the near-unity singlet measurement probability with low visibility, high frequency oscillations at small Δt . (b) Vertical cuts through (a), showing $P_S(\tau_S)$ curves, from which visibilities, V , and nuclear field differences, ΔB_z , are extracted via fits (solid curves) to Eq. (10), for $\Delta t = 150$ s and 300 s. (c) Normalized Fourier amplitudes, A_{FFT} (grayscale), of data in (a). (d) Vertical cuts through (c), for $\Delta t = 150$ s and 300 s following pumping cycle. (e) Overhauser field difference, ΔB_z at $B_{\text{ext}} = 100$ mT (black) and 20 mT (red) as function of time, Δt after pumping, using Eq. 1, which gives $\Delta B_z \sim f_S$ mT/(6.2 MHz). ΔB_z decays faster at lower fields, as expected for spin diffusion.^{3,16} (f) Visibility, V , of S - T_0 oscillations as function of Δt for data in (a) (black), and similar data at $B_{\text{ext}} = 20$ mT (red).

with α and β fit parameters. Figure 2(c) shows the charge relaxation rate, Γ_S [Eq. (9)], exchange, J [Eq. (6)], and singlet admixture, P_{T-S} [Eq. (5)], as functions of detuning, using experimental parameters determined by fits described below.

IV. EXPERIMENT

A 60 s pump-cycle sequence with a ~ 4 MHz repetition rate, ramping through ~ 10 μ eV in ϵ around ϵ_I in 100 ns, was used to prepare a nonequilibrium nuclear spin configuration in the double quantum dot. Immediately after, a probe-cycle sequence was run to extract the nuclear field difference from the S - T_0 precession rates. Following Ref. 11, within each cycle a singlet was prepared in (0,2)

at ϵ_P , separated to $\epsilon_S \sim -700 \mu\text{eV}$ for a time τ_S , then moved to ϵ_M for a measurement time $\tau_M^{\text{max}} \sim 10 \mu\text{s}$. The charge sensor signal, v_{rf} , was integrated over $\sim 300 \text{ ns}$, yielding a single-shot measurement, which was identified as either a singlet or a triplet by comparison to a threshold voltage. For each τ_S , 100 single-shot measurements were performed, with the fraction of singlet outcomes determining P_S , the singlet probability. Figure 3(a) shows P_S as function of τ_S and time, Δt , after the pump-cycle sequence. The separation time, τ_S , is stepped from 1 ns to 100 ns in 80 steps. Resulting sets of 8000 cycles, acquired in 1 s [one column in Fig. 3(a)], are shown for two values of Δt in Fig. 3(b). Measurements taken soon after the pump-cycle sequence, $\Delta t \lesssim 50 \text{ s}$, show $P_S \sim 1$. At somewhat longer times, $50 \text{ s} \lesssim \Delta t \lesssim 300 \text{ s}$, high frequency oscillations can be seen with low visibility. At longer times, $\Delta t \gtrsim 300 \text{ s}$, near-unity oscillations are observed, reflecting S - T_0 precession with frequencies corresponding to equilibrium nuclear field differences, ΔB_z .

Fast Fourier transform (FFT) power spectra of $P_S(\tau_S)$ are shown in Fig. 3(c). Each spectrum has a single, strong peak, as seen in the cuts at $\Delta t = 150 \text{ s}$ and $\Delta t = 300 \text{ s}$ in Fig. 3(d). The peak frequency decreases with increasing Δt , indicating that the Overhauser field gradient, ΔB_z is decreasing following the pump cycle.

Fits of the form

$$P_S(\tau_S) = P_0 + 1/2 V \cos(2\pi f_S \tau_S) \quad (10)$$

to the time-domain data [Fig. 3(a)] are used to extract values for ΔB_z using Eq. (1) and visibility, V . Examples of these fits are shown as solid curves in Fig. 3b. Values for ΔB_z obtained from time-domain fits are consistent with values of FFT peak frequencies [Fig. 3(c)]. For the cut at $\Delta t \sim 150 \text{ s}$ the visibility is $V = 0.2$, and the extracted nuclear field difference is $\Delta B_z \sim 20 \text{ mT}$, while for the cut at $\Delta t \sim 300 \text{ s}$, $V = 0.6$, and $\Delta B_z \sim 6 \text{ mT}$.³⁵ Figures 3(e,f) show ΔB_z and V for the data sets in Fig. 3(a) (time domain) and Fig. 3(c) (frequency domain). Results of a similar pump-probe experiment at lower applied field, $B = 20 \text{ mT}$ is also shown in Figs. 3(e,f). Note that the decay of the field difference with time, Δt , is faster for the 20 mT data, consistent with a nuclear spin diffusion model.^{3,16}

Pump-probe measurements were performed at nine measurement points, ϵ_M . Parametric plots of extracted visibility as a function of ΔB_z are shown in Fig. 4(a) for three of the nine values. Note that for smaller values of ϵ_M , visibility decreases more rapidly with increasing ΔB_z .

To separate the various contributions to visibility, we first define a total visibility, V_T , as the product of V_M , the extrinsic visibility of single-shot readout, whose contributions, such as amplifier noise, are discussed in Ref. 11, and V_J , the intrinsic visibility of S - T_0 precession, reduced by a nonvanishing J at the separation point [Eq. (2)],

$$V_T = V_M V_J, \quad (11)$$

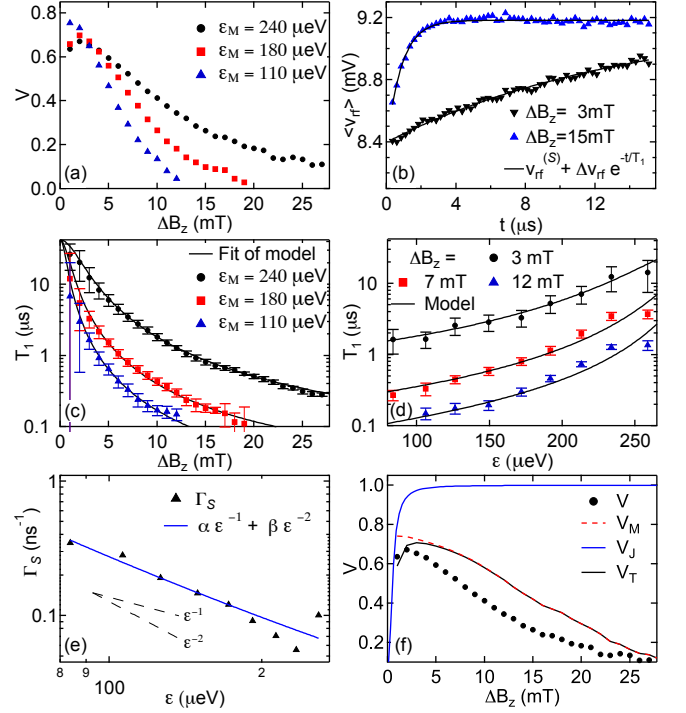


FIG. 4: (Color online) (a) Parametric plot of extracted visibility, V , of S - T_0 precession and nuclear field gradient, ΔB_z , for three values of measurement-point detuning, ϵ_M . (b) rf voltage amplitude, $\langle v_{\text{rf}} \rangle$, as function of time at ϵ_M following separation, for two values of ΔB_z , averaged over an ensemble of 8000 point with separation times τ_S ranging from 1 - 100 ns. Exponential fits with offsets (solid curves, formula in graph) give $T_1 \sim 13 \mu\text{s}$ for $\Delta B_z = 3 \text{ mT}$ and $T_1 \sim 0.8 \mu\text{s}$ for $\Delta B_z = 15 \text{ mT}$. (c) Parametric plot of relaxation time, T_1 , of T_0 state versus Overhauser gradient, ΔB_z . Solid lines are a best fit of Eq. (4) over all values of ϵ_M , with a single set of fit parameters $\Gamma_S(\epsilon_M)$ [see (e)], $\Gamma_T \sim (40 \mu\text{s})^{-1}$, and tunnel coupling, $t_T = 12 \mu\text{eV}$, which determines $J(\epsilon_M)$ via Eq. (6). (d) T_1 as function of detuning ϵ_M , for 3 different ΔB_z . Model (curves) based on Eq. (9) for $\Gamma_S(\epsilon_M)$ with parameters from (e). (e) Singlet relaxation rate Γ_S from fit of Eq. (4) to data in (c,d) along with fit to Eq. (9) (solid line) with fit parameters $\alpha \sim 11 \mu\text{eV ns}^{-1}$ and $\beta \sim 1600 (\mu\text{eV})^2 \text{ ns}^{-1}$. The functional form is consistent with rate contributions from 3D (α) and 2D (β) piezo-electric phonons, see Ref. 33. (f) Visibility, V , from fits to S - T_0 precession data [Fig. 3(b)], for $\epsilon_M = 240 \mu\text{eV}$, along with model visibilities, V_T based on Eq. (11). Single-shot measurement visibility, V_M , is calculated from the measured T_1 and measurement signal-to-noise ratio. The pure singlet precession visibility, V_J , Eq. (2), reflects finite exchange, $J_S \sim 10 \text{ neV} \sim 0.5 \text{ mT}$, at point S.³¹

noting that $V_J \sim 1$ for all but the smallest Overhauser gradients, $\Delta B_z \lesssim 1 \text{ mT}$. V_M is calculated from the experimental parameters following Ref. 11, and depends on the triplet relaxation time, T_1 , at the measurement point. $T_1(\Delta B_z)$ is measured via the charge signal, v_{rf} , with 100 ns time resolution over $\tau_M^{\text{max}} = 4 \mu\text{s}$. After 200 s, the measurement is repeated with 250 ns time resolution over 15 μs , allowing both short and long T_1

regimes to optimally fill the oscilloscope memory. Figure 4(b) shows $\langle v_{\text{rf}} \rangle$ averaged over 8000 probe cycles over a range of τ_{S} values from 1 to 100 ns, as a function of measurement time, τ_{M} . An exponential fit to the decay of $\langle v_{\text{rf}}(\tau_{\text{M}}) \rangle$ from the short-time value $v_{\text{rf}}^{(S)} + \Delta v_{\text{rf}} P_T(0)$ —corresponding to the initial mixture of charge states (0,2) and (1,1)—to the saturating value $v_{\text{rf}}^{(S)}$ yields relaxation times $T_1 \sim 13 \mu\text{s}$ for $\Delta B_z = 3 \text{ mT}$ and $T_1 \sim 0.8 \mu\text{s}$ for $\Delta B_z = 15 \text{ mT}$.

Similar to the visibility, T_1 decreases with increasing ΔB_z [Fig. 4(c)] and decreasing ϵ_{M} [Fig. 4(d)]. To compare the model to the experimental data, the value of $J(\epsilon_{\text{M}})$ is determined by Eq. (6) with the triplet tunnel coupling, $t_T \sim 12 \mu\text{eV}$ as a single fit parameter. The singlet tunnel coupling, $t_S \sim 10 \mu\text{eV}$, is estimated from the detuning, ϵ_{I} , of the S - T_+ resonance.³⁴ The energy detuning, $\epsilon_T \sim 300 \mu\text{eV}$, of the triplet charge transition is determined from dc transport measurements.^{26,27} The fit, together with the measured parameters, yields the ϵ -dependence of exchange energy, $J(\epsilon_{\text{M}})$, shown in Fig. 2(c).

The bare triplet relaxation rate, $\Gamma_T \sim (40 \mu\text{s})^{-1}$, is assumed to be equal for all detunings, an approximation that is justified by the weak dependence of Eq. (4) on Γ_T for $\Delta B_z > 1 \text{ mT}$ and because measured values of T_1 agree with each other within the errors at small ΔB_z . For the singlet charge relaxation rate, $\Gamma_S(\epsilon_{\text{M}})$, one fit parameter is used for each detuning, ϵ_{M} , yielding the values shown in Fig. 4(e). A fit of $\Gamma_S(\epsilon_{\text{M}})$ to the form Eq. (9) gives $\alpha \sim 11 \mu\text{eV ns}^{-1}$ and $\beta \sim 1600 \mu\text{eV}^2 \text{ ns}^{-1}$. At $\epsilon_{\text{M}} \sim 150 \mu\text{eV}$, the contributions from 2D and 3D phonons are about equal, and the fit is in reasonably good agreement with the data. The charge relaxation rates are consistent with the values measured in Ref. 33, when taking into account the difference in tunnel couplings, t_S . Deviations from the form (9) are expected, e.g. due to resonances from finite lengths in the phonon environment.³³

Figure 4(d) shows the model, Eq. (4), with $\Gamma_S(\epsilon_{\text{M}})$ from Eq. (9), using α and β from the fit in Fig. 4(e). Extracted values of α and β are rough estimates, as the functional form of $J(\epsilon_{\text{M}})$, Eq. (6), is only approximate. The detuning dependence of Γ_S , assuming Eq. 9 and using the obtained fit parameters α and β , is shown in Fig. 2(c). Since $\Gamma_S \propto t_S^2$,³³ and roughly $J \propto t_S^2$ (t_T increases with t_S), the first and dominant term in Eq. (4) becomes $\propto \Delta B_z^2/t_S^2$ for $\Delta B_z < J$. Contrary to intuition, a more transparent tunnel barrier yields longer triplet relaxation times, which is beneficial for quantum information processing, where large tunnel couplings enable fast operations.^{7,14}

The magnitude of the applied magnetic fields changes the overall rate of decay of nuclear polarizations [Figs. 3(e,f)]. However, the parametric dependence of visibility and relaxation time on Overhauser gradient do not change with applied magnetic field, B , as shown in Fig. 5.

Finally, we consider the effect of finite pulse rise times

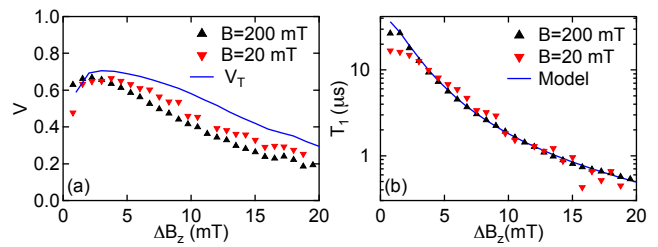


FIG. 5: (Color online) (a) Parametric plot of measured visibility, V [Fig. 3(f)], versus nuclear field difference, ΔB_z [Fig. 4(e)] for applied fields of 200 mT and 20 mT. Model of total visibility, V_T , using measured relaxation time, T_1 [Fig. 3(f)]. (b) Triplet relaxation time, T_1 , as function of nuclear field difference, ΔB_z , along with the model, using Eq. (4). The ΔB_z dependence of V and T_1 does not depend on the applied magnetic fields.

on visibility. We observe that the model for total visibility, V_T , based on Eq. (11), using measured values of T_1 , overestimates the measured visibility except at the lowest values of ΔB_z [Fig. 5(a)]. We attribute this deviation to finite ramp rates of the separation and return pulses, which we can account for phenomenologically by including a ramp-rate-dependent factor V_R in the visibility model,

$$V = V_R V_T. \quad (12)$$

We investigated V_R by including a deliberate ramp time, τ_R , to the probe cycle. Following a 60 s, 4 MHz pump-cycle sequence, a prepared singlet was separated to point S over the ramp time, τ_R , then ramped to point M, also over τ_R . Resulting visibilities are shown in Fig. 6(a), together with the model V_T based on the measured T_1 using Eq. (11). Note that T_1 itself does not depend on τ_R , as shown in Fig. 6(b). The ramp-rate factor, V_R , extracted by dividing the measured visibility by the model total visibility, $V_R = V/V_T$, is shown in Fig. 6(c). With longer ramp times, V_R decreases more rapidly with increasing ΔB_z . Due to the finite rise time of the pulses, the data without intentional ramp time has an estimated ramp time, $\tau_R \sim 3 \text{ ns}$, and $V_R < 1$, at finite nuclear field differences.

To further characterize the dependence V_R on ΔB_z , we define $B_{90\%}$ as the maximum gradient for which $V_R > 0.9$. A phenomenological exponential fit [Fig. 6(c)] gave values for $B_{90\%}$ that increase roughly linearly with increasing ramp rate, $1/\tau_R$ [Fig. 6(d)]. We conclude that the visibility factor V_R for the probe-cycle without an intentional ramp can similarly be attributed to the finite pulse rise time, limited by the bandwidth of the experimental set-up.

V. CONCLUSIONS

An enhanced Overhauser field gradient results from an electron-nuclear spin pumping cycle under all conditions

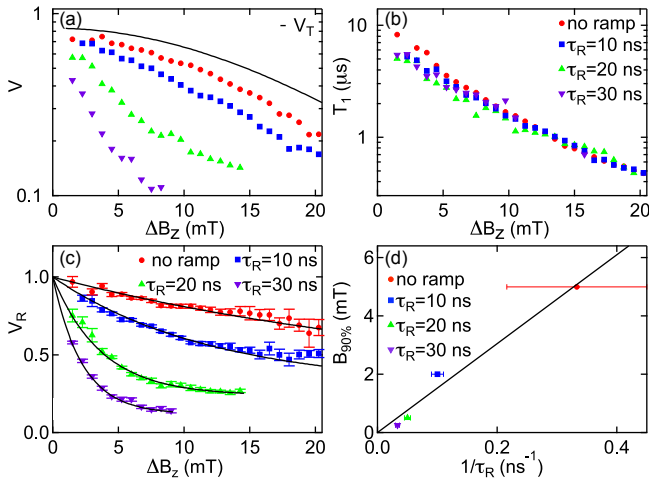


FIG. 6: (Color online) (a) Parametric plot of visibility, V , of S - T_0 precession as a function of field gradient, ΔB_z , for ramp times τ_R [legend in (b) and (c)] from initial singlet to separation point S and back to measurement point M, along with model total visibility, V_T (solid curve) based on measured T_1 values. (b) Relaxation time, T_1 , as function of nuclear field difference, ΔB_z , shows no dependence on ramp time, τ_R . (c) Ramp-rate visibility factor $V_R = V/V_T$ as function of ΔB_z for different τ_R , along with exponential fits, $V_R = e^{-\Delta B_z/B_W} + V_0$ ³⁶ (d) $B_{90\%}$, the nuclear field difference for which $V_R = 0.9$, as function of inverse ramp duration, $1/\tau_R$. Without an intentional ramp, $\tau_R \sim 3$ ns.

investigated. The resulting difference in z components of Overhauser fields reduces the relaxation time of the $m = 0$ triplet state during measurement, lowering the

visibility of single-triplet qubit readout. Bandwidth limited pulses further reduce readout fidelity. Visibility reduction due to field gradients appears to be the likely explanation for the experiments discussed in Ref. 17. For applications using magnetic or Overhauser field gradients^{12,14} it is desirable to design the exchange interaction to allow long triplet lifetimes. In the presence of a magnetic field difference, the device should be tuned to a large inter-dot tunnel coupling with a measurement point chosen at large detuning, near the T_0 anticrossing, where exchange protects the triplet, while the charge relaxation rate is small. To mitigate errors from finite pulse rise times, an initialization of the qubit via adiabatic loading of $|\uparrow\downarrow\rangle$, followed by a $\pi/2$ pulse, may be preferable over the diabatic initialization used here and in Refs. 3,7,14. We would like to point out that the results of this paper do not imply a short relaxation time of the qubit while it is operated in the $(1, 1)$ state, where T_1 is much longer and expected to be independent of magnetic field gradients.³⁷

Acknowledgments

We acknowledge funding from IARPA/MQCO program and DARPA/QUEST program. Device fabrication used Harvard's Center for Nanoscale Systems (CNS), supported by the National Science Foundation under ECS-0335765. We thank D.J. Reilly, J.M. Taylor, and S. Foletti for useful discussion.

*These authors contributed equally to this work.

† Present address: 2nd Institute of Physics C, RWTH Aachen University, DE-52074 Aachen, Germany

- ¹ L. Chirulli and G. Burkard, Adv. in Phys., **57**, 225 (2008).
- ² R. de Sousa, Top. Appl. Phys. **115**, 183 (2009).
- ³ D. J. Reilly, J. M. Taylor, E. A. Laird, J. R. Petta, C. M. Marcus, M. P. Hanson, and A. C. Gossard, Phys. Rev. Lett. **101**, 236803 (2008).
- ⁴ D. Klauser, W. A. Coish, D. Loss, Adv. Solid State Phys. **46**, 17 (2007).
- ⁵ R. Hanson, L. P. Kouwenhoven, J. R. Petta, S. Tarucha, and L. M. K. Vandersypen, Rev. Mod. Phys. **79**, 1217 (2007).
- ⁶ J. Levy, Phys. Rev. Lett. **89**, 147902 (2002).
- ⁷ J. R. Petta, A. C. Johnson, J. M. Taylor, E. A. Laird, A. Yacoby, C. M. Marcus, M. P. Hanson, and A. C. Gossard, Science **309**, 2180 (2005).
- ⁸ H. Bluhm et al., Nature Phys. **7**, 109 (2010).
- ⁹ C. Barthel et al., Phys. Rev. Lett. **105**, 266808 (2010).
- ¹⁰ A. C. Johnson, J. R. Petta, J. M. Taylor, A. Yacoby, M. Lukin, C. M. Marcus, M. P. Hanson, and A. C. Gossard, Nature **435**, 925 (2005).
- ¹¹ C. Barthel, D. J. Reilly, C. M. Marcus, M. P. Hanson, and A. C. Gossard, Phys. Rev. Lett. **103**, 160503 (2009).
- ¹² M. Pioro-Ladrière, Y. Tokura, T. Obata, T. Kubo, and S. Tarucha, Appl. Phys. Lett. **90**, 024105 (2007).
- ¹³ T. Obata, M. Pioro-Ladrière, Y. Tokura, Y.-S. Shin, T. Kubo, K. Yoshida, T. Taniyama, and S. Tarucha, Phys. Rev. B **81**, 085317 (2010).
- ¹⁴ S. Foletti, H. Bluhm, D. Mahalu, V. Umansky, and A. Yacoby, Nature Physics, **5**, 903 (2009).
- ¹⁵ J. R. Petta, J. M. Taylor, A. C. Johnson, A. Yacoby, M. D. Lukin, C. M. Marcus, M. P. Hanson, A. C. Gossard, Phys. Rev. Lett. **100**, 067601 (2008).
- ¹⁶ D. J. Reilly, J. M. Taylor, J. R. Petta, C. M. Marcus, M. P. Hanson, and A. C. Gossard, Phys. Rev. Lett. **104**, 236802 (2010).
- ¹⁷ D. J. Reilly, J. M. Taylor, J. R. Petta, C. M. Marcus, M. P. Hanson, and A. C. Gossard, Science **321**, 817 (2008).
- ¹⁸ Arne Brataas and Emmanuel I. Rashba, Phys. Rev. B **84**, 045301 (2011).
- ¹⁹ G. Ramon and X. Hu, Phys. Rev. B **75**, 161301 (2007).
- ²⁰ H. Ribeiro and G. Burkard, Phys. Rev. Lett. **102**, 216802 (2009).
- ²¹ M. Stopa, J. J. Krich, and A. Yacoby, Phys. Rev. B **81**, 041304(R) (2010).
- ²² M. Gulland, J. J. Krich, J. M. Taylor, H. Bluhm, B. I. Halperin, C. M. Marcus, M. Stopa, A. Yacoby, and M. D. Lukin, Phys. Rev. Lett. **104**, 226807 (2010).

- ²³ The leverarms for gate voltages V_L and V_R are approximately equal in the measured device.
- ²⁴ C. Barthel, M. Kjaergaard, J. Medford, M. Stopa, C. M. Marcus, M. P. Hanson, and A. C. Gossard, Phys. Rev. B **81**, 161308(R) (2010).
- ²⁵ D. J. Reilly, C. M. Marcus, M. P. Hanson, and A. C. Gossard, Appl. Phys. Lett. **91**, 162101 (2007).
- ²⁶ A. C. Johnson, J. R. Petta, C. M. Marcus, M. P. Hanson, and A. C. Gossard, Phys. Rev. B **72**, 165308 (2005).
- ²⁷ W. G. van der Wiel, S. D. Franceschi, J. Elzerman, T. Fujisawa, S. Tarucha, and L. P. Kouwenhoven, Rev. Mod. Phys. **75**, 1 (2003).
- ²⁸ J. M. Taylor, J. R. Petta, A. C. Johnson, A. Yacoby, C. M. Marcus, and M. Lukin, Phys. Rev. B **76**, 035315 (2007).
- ²⁹ Equations (16) and (17) of Ref. 28 contain a sign error resulting in the lower branch being positive and the upper branch being negative for all ϵ . We invert the sign in our analysis.
- ³⁰ W. A. Coish and D. Loss, Phys. Rev. B **72**, 125337 (2005).
- ³¹ E. A. Laird, J. R. Petta, A. C. Johnson, C. M. Marcus, A. Yacoby, M. P. Hanson, and A. C. Gossard, Phys. Rev. Lett. **97**, 4 (2006).
- ³² J_S , estimated to be $J_S \sim 10 \text{ neV} \pm 5 \text{ neV}$, from the drop of V_J at the lowest measured field differences, results in a shifted frequency $f_S^* = \sqrt{f_S^2 + (J_S^2/h)^2}$, a negligible correction at the relevant frequencies.
- ³³ T. Fujisawa, T. H. Oosterkamp, W. G. van der Wiel, B. W. Broer, R. Aguado, S. Tarucha, and L. P. Kouwenhoven, Science **282**, 932 (1998).
- ³⁴ At ϵ_I , the exchange energy, J_S , is equal to the Zeeman energy of T_+ . Comparison with $J_S = t_S^2/(\epsilon_I - \sqrt{4t_S^2 + \epsilon_I^2})$, from Ref. 28, yields an estimate of t_S .
- ³⁵ Other parameters are, $P_0 = 0.6$ for $\Delta t = 150 \text{ s}$, and $P_0 = 0.4$ for $\Delta t = 300 \text{ s}$.
- ³⁶ For no ramp, $V_0 \sim 0.3$, $B_W \sim 31 \text{ mT}$; for $\tau_R = 10 \text{ ns}$, $V_0 \sim 0.3$, $B_W \sim 12 \text{ mT}$; for $\tau_R = 20 \text{ ns}$, $V_0 \sim 0.2$, $B_W \sim 4 \text{ mT}$; for $\tau_R = 30 \text{ ns}$, $V_0 \sim 0.1$, $B_W \sim 2 \text{ mT}$. In Fig. 6(d), the slope of the linear fit is $\sim 15 \text{ mT ns}$.
- ³⁷ S. Amasha, K. MacLean, I. P. Radu, D. M. Zumbuhl, M. A. Kastner, M. P. Hanson, and A. C. Gossard, Phys. Rev. Lett. **100**, 046803 (2008).